Atmos. Meas. Tech. Discuss., 5, 8995–9020, 2012
www.atmos-meas-tech-discuss.net/5/8995/2012/
doi:10.5194/amtd-5-8995-2012
© Author(s) 2012. CC Attribution 3.0 License.

Atmospheric Measurement Techniques Discussions

This discussion paper is/has been under review for the journal Atmospheric Measurement Techniques (AMT). Please refer to the corresponding final paper in AMT if available.

A cavity ring-down spectroscopy sensor for measurements of gaseous elemental mercury – Part 1: Development for high time resolution measurements in ambient air

A. Pierce[1], **D. Obrist**[1], **H. Moosmüller**[1], **X. Faïn**[1,2], **and C. Moore**[1]

[1]Desert Research Institute, Division of Atmospheric Sciences, Reno, NV, USA
[2]Laboratoire de Glaciologie et Géophysique de l'Environnement, St Martin d'Hères, France

Received: 6 November 2012 – Accepted: 27 November 2012 – Published: 21 December 2012

Correspondence to: A. Pierce (ashley.pierce@dri.edu)

Published by Copernicus Publications on behalf of the European Geosciences Union.

Abstract

The ability to make high time resolution measurements of gaseous elemental mercury (GEM) concentrations in air is imperative for the understanding of mercury cycling. Here we describe further development and field implementation of a laboratory prototype pulsed cavity ring-down spectroscopy (CRDS) system for high time resolution, continuous and automated measurement of GEM concentrations in ambient air. In particular, we present use of an external, isotopically enriched Hg cell for automated wavelength locking and wavelength stabilization to maintain laser wavelength on the peak of GEM absorption line in ambient air. We further describe implementation of differential absorption measurements using a piezoelectric tuning element that allows for continuous accounting of system baseline extinction losses needed to calculate GEM absorption coefficients. Data acquisition systems and software programs were modified to acquire high-speed ring-down data at 50 Hz repetition rate as well as process and analyze data in real time. The system was installed in a mobile trailer, and inlet systems and temperature controls were designed to minimize effects of changes in ambient air temperature and ozone (O_3) concentration. Data that identify technical challenges and interferences that occurred during measurements, including temperature fluctuations, interferences by ambient O_3 and drifts in frequency conversion efficiencies are discussed. Successful development of a CRDS system capable of measuring ambient air GEM concentrations with high time resolution is based on minimizing these interferences.

1 Introduction

Mercury (Hg) is a highly toxic pollutant with an important presence in the atmosphere due to its high volatility (Schroeder and Munthe, 1998) and global atmospheric distribution. Atmospheric cycling is particularly important because deposition is the primary source of Hg to many remote ecosystems (Fitzgerald et al., 1998; Lindberg et al., 2007;

AMTD
5, 8995–9020, 2012

Rothenberg et al., 2010). Based on currently available analytical techniques, three major forms of atmospheric Hg are being speciated: gaseous elemental mercury (GEM), gaseous oxidized mercury (GOM), and particulate-bound mercury (PHg). GEM generally represents more than 90 % of the atmospheric Hg mass, is relatively inert, and has low solubility in water. As a result, GEM has a long residence time in the atmosphere (5 to 24 months) and can be transported over long distances (Schroeder and Munthe, 1998; Lamborg et al., 2002; Slemr et al., 1985; Swartzendruber et al., 2006). GOM and PHg have much shorter atmospheric residence times and are considered to be local or regional pollutants (Swartzendruber et al., 2006; Schroeder and Munthe, 1998; Shia et al., 1999). The most relevant Hg exposure occurs after deposition when Hg can be converted into methylmercury by bacteria (Harris et al., 2007) and can bioaccumulate in marine and terrestrial species to levels known to cause health problems in wildlife and humans (Zhang et al., 2009; Clarkson and Magos, 2006). Accurate quantification of sources and sinks of atmospheric Hg is needed for regulatory measures to mitigate current and future atmospheric Hg loads as well as negative impacts on humans, wildlife, and ecosystems.

Existing technologies for measuring the dominant atmospheric form of Hg, GEM, generally require several minutes (e.g. 2.5 min) of sampling time and multiple liters of air to accurately determine the concentration of a single sample (Landis et al., 2002; Lyman et al., 2010). This slow temporal response complicates quantification of atmospheric Hg dynamics as we are currently not able to quantify high frequency fluctuations of GEM concentrations that may correspond to sources, sinks, and chemical transformations as is possible with other pollutants such as ozone (O_3) and carbon monoxide (CO). For example, Fig. 1a shows an ambient air time series of GEM and CO measured at Storm Peak Laboratory in the high Rocky Mountains, Colorado, in winter of 2006/2007 (Obrist et al., 2008); Fig. 1b shows a Fourier spectral transformation of the GEM data which lacks a drop in power spectrum at the Nyquist frequency (1.67×10^{-3} Hz), indicating that the available 5 min time resolution of the analyzer did not account for concentration fluctuations that occurred at higher time resolutions.

AMTD
5, 8995–9020, 2012

A fast-response sensor likely would facilitate enhanced characterization of sources, sinks, and oxidation pathways and kinetics – such as during atmospheric mercury depletion events (Fritsche et al., 2008; Deanna et al., 2006; Donohoue et al., 2005; Arya, 2001).

Faïn et al. (2010) describe a laboratory prototype based on cavity ring-down spectroscopy (CRDS; Sect. 2.1.) that uses high-reflectivity mirrors to create long absorption path lengths in a compact cell (1 m; Sect. 2.2.). The authors presented manual wavelength scans including the Hg absorption wavelength of 253.65 nm to characterize GEM concentrations in the laboratory using Hg-free air (i.e. charcoal-filtered air) spiked with GEM to reach concentrations between 0.2 and 573 $ng\,m^{-3}$ (Faïn et al., 2010). In addition, they presented preliminary measurements of GEM in ambient air and defined potential interferences by ambient-air constituents such as O_3 and particulate matter that show absorption in the same wavelength region as GEM.

Here, we describe refinements to the laboratory prototype documented by Faïn et al. (2010), and development of that prototype into a field-deployable, mobile sensor for high time resolution measurement of GEM in ambient air. We explain in detail (Sect. 3) how laser wavelength is automatically and reliably positioned ("locked") onto the peak Hg absorption line using an external, Hg-filled cell; implementation of differential absorption measurements to continuously correct for baseline system extinction by alternating measurements on the Hg absorption line ("online") and an adjacent wavelength where no Hg absorption occurs ("offline"); automation of data acquisition and real-time signal processing at 50 Hz laser pulse repetition rate for continuous CRDS absorption measurements; as well as set-up and configuration of the system in a mobile platform to allow in situ field measurements. Preliminary ambient air data and sensitivity are reported and particular challenges using the differential absorption technique and operating the system in a mobile platform also are discussed.

AMTD
5, 8995–9020, 2012

2 Pulsed cavity ring-down spectroscopy and the previous laboratory prototype

2.1 Cavity ring-down spectroscopy – overview of theory

Pulsed cavity ring-down spectroscopy is an absorption technique using high-reflectivity mirrors positioned at both ends of a high-finesse measurement cavity. A small fraction of the power of each laser pulse is coupled into the cavity through one of its mirrors where it bounces between the two mirrors; multiple reflections of the laser pulse produce long path lengths for absorption measurements leading to greater sensitivity compared to standard absorption measurements (Jongma et al., 1995; Spuler et al., 2000; Atkinson, 2003). In addition, the use of a short cavity allows for small sample volumes (Moosmüller et al., 2005). The laser pulse energy introduced into the cavity decays exponentially with time due to extinction and reflection losses within the cavity. CRDS measures total extinction in the cavity, which is the sum of mirror losses, scattering and absorption losses due to particles and gases inside the cavity (Tao et al., 2000; Moosmüller et al., 2005; Atkinson, 2003). The power in the cavity can be quantified by the current signal S_t of a photomultiplier tube exposed to the light leaking out of the cavity through the second mirror. Equation (1) shows how the signal S_t decays with time due to various system components:

$$S_t = S_0 e^{-\alpha c t} = S_0 e^{-[(\alpha_{Hg}+\alpha_{BG}+\alpha_M)\cdot ct]}, \quad (1)$$

where S_0 is the signal at $t = 0$; α is the sum of the wavelength-dependent Hg absorption coefficient α_{Hg}, a background extinction coefficient α_{BG} (gaseous and particulate absorption and scattering), and a mirror extinction term α_M; c is the speed of light; and t is time. If all losses other than those occurring from GEM (α_{BG} and α_M, termed baseline losses here) can be reliably quantified, absorption losses by GEM (α_{Hg}) can be calculated by measuring total extinction losses. In our system, the extinction loss through time ($\sim 3\,\mu s$ signal decay time) is quantified using exponential fits of the signal for each pulse (Wheeler et al., 1998).

AMTD
5, 8995–9020, 2012

2.2 The laboratory prototype

The system we have further refined operates at UV laser wavelengths at and near peak absorption for GEM (253.65 nm; Spuler et al., 2000). These wavelengths are created by a Quanta Ray, Q-switched Nd:YAG pump laser (Newport-Spectra-Physics, Mountain View, CA, USA) operating at a fundamental wavelength of 1064 nm with a frequency-tripled output of 355 nm. This laser pumps a dye laser (model Sirah Cobra, Sirah Laser- und Plasmatechnik GmbH, Kaarst, Germany) to generate a frequency-doubled output tunable between 215 and 280 nm. Short (5 ns) laser pulses are directed into a 1 m long closed-path cavity built with two 99.895 % reflectivity mirrors (MLD Technologies, Mountain View, CA, USA). Using an external, low pressure Hg cell system and two photodiodes (PDs) (DET10M, Thorlabs, Newton, NJ, USA; Sect. 3.1) the laser wavelength is determined relative to the Hg absorption line. Manual scans were performed to characterize the Hg absorption spectra. Measurements of GEM concentrations were performed by scanning the laser wavelength to one of five resolvable isotopes of Hg (Sect. 3.1 and Fig. 2a) for 10 s and then scanning off the absorption line for another 10 s to quantify system baseline extinction.

3 Automated, high time resolution measurements on a mobile platform

3.1 Wavelength locking / stabilization of the laser system

Exact positioning and control of the laser wavelength is a critical requirement for replicable and reliable spectroscopic measurements with a tunable laser system. For instance, in the original design of our system, the dye laser wavelength (tunable between 215 and 280 nm) was obtained from the mechanical position of its tuning grating. Since this was a mechanical estimation and not an actual measurement of wavelength, it was relatively inaccurate (within ±0.03 nm according to Sirah) and insufficient to position

AMTD
5, 8995–9020, 2012

the laser wavelength onto the narrow Hg absorption line (0.005 nm Full Width at Half Maximum (FWHM) at atmospheric pressure, Fig. 2a).

To more accurately control the laser wavelength, we started using an external Hg cell as a wavelength reference to control and position laser wavelength with high accuracy relative to the wavelength of the Hg absorption line. Specifically, a small fraction of the laser energy was deflected from the main laser beam (that continued into the measurement cavity) using a fused silicate plate (ESCO corp., Oak Ridge, NJ, USA). This beam was further split into two paths with near-equal beam power using a 1 : 1 UV beam splitter (Edmund Optics Inc., Barrington, NJ, USA); one path passed through the external Hg cell after which the transmitted power was quantified with a photodiode detector (PD_{Hg}; DET10M, Thorlabs, Newton, NJ, USA); the second path without the Hg cell was used as reference, and its beam power was measured with a second photodiode detector (PD_{ref}). A schematic of the system is shown in Fig. 2b. Photodiode signals were then routed into boxcar amplifiers (SR250, 2 ns Gated Integrator, Stanford Research Systems, Sunnyvale, CA, USA) where gate parameters were set to reduce the influence of background noise on the low-duty cycle signals.

The resulting DC voltage signals were acquired with a data acquisition module (DAQ; National Instruments, Austin, TX, USA) at 50 Hz and routed to a LabVIEW program (National Instruments, Austin, TX, USA) for data processing. Using the ratio of the two photodiode signals provided a sensitive signal for positioning the laser wavelength: Fig. 2a shows the ratios of the two photodiode voltage signals (PD_{Hg}/PD_{ref}; plotted on a normalized y-scale to compare different scans) for wavelength scans over the Hg absorption spectrum. Low PD_{Hg}/PD_{ref} ratios are indicative of the strongest absorption of Hg, when laser wavelength equals the peak wavelength of the Hg absorption spectrum. Note that the laser linewidth at 253.65 nm is ~0.9 GHz (0.00019 nm), which is much narrower than the FWHM (0.005 nm) of the GEM absorption line.

We tested several external Hg cells made of 50 mm long, 8 mm diameter fused quartz tubes with two high quality fused silica windows attached at 15° angles (Fig. 2c, Thorlabs, Newton, NJ, USA). A 10 mm long stem that protrudes from the external Hg cell

AMTD
5, 8995–9020, 2012

was filled with a small drop of liquid Hg. The high vapor pressure of Hg (0.25 Pa at 25 °C, Schroeder et al., 1991) resulted in high vapor concentrations inside the cell (2.1×10^7 ng m^{-3} at 25 °C, Huber et al., 2006). Such high GEM concentrations inside the Hg cells (compared to ambient air GEM levels of about 1.5 to 1.7 ng m^{-3}; Spuler et al., 2000) were easily detected and used to position the laser wavelength of the system. Figure 2a shows the absorption spectrum of an Hg cell filled with metallic GEM at ambient pressure (~ 80 kPa within cell; green line); the spectrum of an Hg cell filled with metallic Hg under low pressure (1.33×10^{-5} Pa within cell; blue line); and the spectrum of an Hg cell filled with an isotopically-enriched, metallic ^{200}Hg (94 % + isotopic purity) under low pressure (1.33×10^{-5} Pa within cell; red line). In the low-pressure Hg spectrum (blue line), five of seven known stable Hg isotopes (Schroeder and Munthe, 1998; Spuler et al., 2000) can be seen as individual hyperfine structures, which are commonly observed when atmospheric pressure broadening is eliminated (Anderson et al., 2007; Spuler et al., 2000; Schweitzer, 1963). Differences between the external Hg cell at ambient pressure (green line) and low pressure (blue line) resulted from collisions of Hg atoms with air molecules, shortening their radiative lifetime or resulting in a phase shift and causing collision-induced/pressure broadening of the absorption line (Demtröder, 2003). The absorption spectrum of the low-pressure, isotopically-enriched, metallic ^{200}Hg cell (red line) was much narrower than the "regular" metallic GEM and had a single, well-defined peak corresponding to absorption by the ^{200}Hg isotope, which is the second most abundant stable Hg isotope with a mole fraction of 0.23 (Spuler et al., 2000). The peak of the ^{200}Hg absorption corresponded well to the peak of the ambient-pressure GEM absorption line that was present in the measurement cavity when operated under ambient air conditions. Therefore, we used the ^{200}Hg low-pressure cell to exactly position and control laser wavelength during measurements.

Positioning and locking (i.e. maintaining) the laser wavelength to the peak absorption of the ^{200}Hg cell was automated with a custom LabVIEW control program. Because temperature changes and other mechanical instabilities caused slight drifts in laser

AMTD
5, 8995–9020, 2012

wavelength, we implemented a set of commands to correct for these. The program minimized the PD_{Hg}/PD_{Ref} ratio in order to remain at the peak of mercury absorption. This was accomplished by changing the laser wavelength by small increments (0.0002 nm) using the grating tuning element of the laser (Faïn et al., 2010). If moving in one direction caused a decrease in PD_{Hg}/PD_{ref} ratios (i.e. moving toward the peak absorption), the program was set to continue changing wavelengths in that direction; if PD_{Hg}/PD_{ref} ratios increased, however, the program would switch the direction of the grating tuning and the wavelength would move back toward peak ^{200}Hg absorption. A time average function was used to implement a 4 s moving average to avoid unnecessary wavelength changes due to noise. For real-time operation, only every second laser pulse was used for the wavelength-locking procedure due to the implementation of differential wavelength measurements (Sect. 3.2). Using this approach, we successfully positioned and maintained (i.e. locked) the laser wavelength to the ^{200}Hg absorption line, and analysis of PD_{Hg}/PD_{ref} ratios indicated that the laser wavelength remained within ±0.08 nm during operation.

3.2 Differential absorption measurements

With CRDS, total extinction losses that occur in the cavity are measured. In order to separate GEM absorption (α_{Hg}) from other system extinction losses, all other signal losses in the cavity must be determined (α_{BG} and α_{M}; Eq. 1). Most spectroscopy techniques use differential absorption measurements to correct for baseline losses, and different methods are employed to do so. For example, differential measurements can be achieved by consecutive measurement of spectral extinction losses with and without the compound of interest present (e.g. by removing (scrubbing) the compound of interest from the sample prior to a measurement) or employing measurements in two parallel extinction cells where the compound of interest is scrubbed from one sample stream such as used in atmospheric O_3 monitors (e.g. Model 205, 2B Technologies, Boulder, CO, USA) or infrared CO_2 gas analyzers (e.g. Model LI 7000, LI-COR Inc., Lincoln, NE, USA).

AMTD
5, 8995–9020, 2012

A major challenge in employing differential GEM measurements in ambient air is that full removal of GEM from the sampling stream is extremely difficult without also removing other ambient air compounds that absorb at the 253.65 nm wavelength (see also Sect. 3.4). Tests in our laboratory have shown that most removal mechanisms for GEM also partially remove O_3 from the sample stream (Part 2; Pierce et al., 2012); hence, baseline measurements would account for air devoid of both GEM and O_3, and differential measurements would result in a combination of GEM and O_3 concentrations. Further, absorption by O_3 in ambient air is large compared to that of GEM, in part because ambient air O_3 levels are about five orders of magnitude (20–50 ppb) higher than GEM (~ 200 ppq). Note that Hg is reported to have an absorption cross section of 3.3×10^{-14} cm^2 mol^{-1} at 254 nm (Jongma et al., 1995; Edner et al., 1989; Spuler et al., 2000), larger than O_3 which has an absorption cross section of 1.2×10^{-17} cm^2 mol^{-1} at 254 nm (Griggs, 1968; Inn and Tanaka, 1953; Molina and Molina, 1986; Mauersberger et al., 1986). Conventional gold amalgamation techniques, such as those employed in the commercially-available Tekran 2537 analyzers, pre-concentrate GEM onto a gold trap and consecutively analyze GEM in a stream of inert carrier gas (argon) to avoid interferences by O_3 and other compounds (Tekran, 2009).

For our analyzer, we implemented differential extinction measurements using high-frequency wavelength tuning, thereby taking advantage of the uniquely narrow Hg absorption line. A piezoelectric tuning element located in the dye laser allows detuning of the laser wavelength (by ~ 0.003 nm, as currently implemented) at the laser pulse repetition rate (i.e. 50 Hz) from the wavelength at which the laser is positioned and locked by the grating tuning (Sect. 2.1). Hence, the piezoelectric tuning element allows alternating laser wavelengths on a pulse-by-pulse basis from the peak Hg absorption line (called "online") to an area directly adjacent (either to a higher or lower wavelength, called "offline"), thereby providing pairs of differential online and offline measurements at 25 Hz repetition rate. To assure synchronization of the pulses emitted by the Nd:YAG laser and the piezoelectric tuning position, a piezo output signal triggers the lamp of the Nd:YAG pump laser to fire. GEM is uniquely suited for such

AMTD
5, 8995–9020, 2012

differential online and offline extinction measurements due to its very narrow absorption line (FWHM 0.005 nm). Hg is the only atmospheric constituent that occurs in the troposphere in elemental form and for which the transition to an excited state (6^1S_0 to 6^3P_1) is not spread across a large number of rotational and vibrational transitions as it is for molecular constituents (Spuler et al., 2000; Edner et al., 1989). Detuning of the laser wavelength by such a small increment (0.003 nm) likely does not change absorption losses of other ambient air constituents.

3.3 Signal acquisition and processing for real-time measurements

In our system, energy from laser pulses in the cavity leaks out through the back mirror attached to the cavity where the signals are captured by a photomultiplier tube (PMT; Model H6780; Hamamatsu, Japan). A CompuScope data acquisition card (CompuScope 12100, GaGe, Lockport, Illinois, USA) is used to digitize the analogue signal, which is then processed in real time by our custom LabVIEW CRDS program. The exponential ring-down of each laser pulse (which occurs at 50 Hz pulse repetition rate) is quantified by 200 measurements taken with an acquisition rate of $1\,\mathrm{MS\,s^{-1}}$. Each acquisition is triggered by the laser Q-switch trigger signal so that signal acquisition is synchronized with laser pulses. Since the first few data points of each ring-down signal show non-exponential decay, possibly caused by an incomplete match between transverse beam and cavity modes, we eliminate the first 15 points of each ring-down. The program then performs an exponential fit to each decay using the non-linear Levenberg–Marquardt method (Press et al., 1986). The three fitting parameters (initial and baseline signal and extinction coefficient α) are exported and saved to a data file.

Because of the high frequency differential tuning/detuning of the laser wavelength (Sect. 3.1), online extinction measurements need to be separated from offline measurements; for this, we use the second channel of the CompuScope acquisition card to read the position of the piezoelectric tuning element (a sinusoidal analog wave with the apex of the sinus curve representing the online signal and the trough representing

AMTD
5, 8995–9020, 2012

the detuned offline signal). The piezo position is recorded in the data file with extinction measurements to allow processing of both online and offline measurements. Both extinction measurements also are continuously graphed during operation so that differential measurements are visible on a screen during real-time measurements (Fig. 3).

3.4 Set-up of measurement system in mobile measurement platform

We installed the CRDS system in a 4.3 × 2.4 m footprint mobile trailer (Fig. 4a) for field deployment. Several modifications to the system and the trailer were required to achieve this. First, the optical components of the system were mounted on a mobile optical table to ensure stability of optical paths (Fig. 4b, c) as well as to allow the system to be moved into the trailer. Second, electrical power was distributed throughout the trailer to power all components of the system. Third, an external chiller was connected to the trailer to allow water cooling of the Nd:YAG laser. Fourth, an air conditioner was added to maintain a stable temperature in the trailer. Fifth, the cavity was thermally insulated using a foam box to further minimize temperature drifts in and around the measurement cavity (Sect. 4.1).

Sample inlets to the trailer consisted of 6.35 mm OD Teflon® tubing and 0.2 µm pore size Teflon filters. We also directed air flow through two ovens to thermally decompose O_3 in ambient air (see O_3 interference issues in Sect. 4.2). We used the ovens of a Tekran speciation unit (Model 1130 and 1135, Tekran Inc., Toronto, Canada) whereby annular denuder and particulate trap glassware (not coated and without a filter, but packed with quartz chips to increase surface area) were heated to 500 °C during measurements. Use of the ovens effectively removed O_3 during ambient air measurements to below the detection limit of an Ozone Monitor (higher of 1.0 ppbv or 2 %; Model 205, 2B Technologies, Boulder, CO, USA) placed after the cavity. Flow through the cavity was set to rates variable up to 10 l min^{-1} using a flow meter (Aalborg, Orangeburg, NY, USA) and external pump.

AMTD
5, 8995–9020, 2012

3.5 Preliminary ambient air measurements

Ambient air measurements and results are fully discussed in Part 2 of this paper (Pierce et. al. 2012) but preliminary data for one day of measurements are discussed here. Calculated GEM concentrations for ambient air measurements showed highly linear relationships when compared to the Tekran 2537B mercury vapor analyzer. Figure 5 shows 1.5 h of measurements on 19 July 2012 in ambient air at 2.5 min time resolution. We demonstrated good agreement with the Tekran analyzer in terms of magnitude of concentration though our concentrations at ambient levels are not as stable as the Tekran. We calculated sensitivity (3 × standard deviation) based on this ambient air run as 0.35 ng m^{-3} at 5 min time resolution. This sensitivity is not as low as currently used commercial analyzers (such as the Tekran 2537 analyzer: about 0.1 ng m^{-3} at 5 min time resolution); however, it demonstrates the first time that ambient air Hg levels in the range of 1.5–1.7 ng m^{-3} were able to be measured by a CRDS system.

4 Challenges during real-time ambient air measurements

4.1 Temperature fluctuations

Although inlet air temperatures were preheated by external ovens and the trailer was temperature-controlled by an air conditioning unit, we detected significant temperature fluctuations (mainly related to the on-and-off cycles of the trailer air conditioning) inside the cavity during measurements. These fluctuations affected the absolute extinction and differential extinction during measurements. Figure 6a shows how a cyclical fluctuation of temperature affected online and offline extinction during ambient-air measurements; most importantly, however, the temperature fluctuations also affected the differential extinction (between online and offline signals), and Fig. 6b demonstrates the behavior of the differential extinction when there were temperature fluctuations. There was a slight delay in cavity response to temperature changes, which we suspect

AMTD
5, 8995–9020, 2012

was due to the temperature-sensitive element(s) of the cavity showing a different time response to temperature changes than the temperature sensor located in the sample line just after the cavity. To solve the issue, we constructed a foam enclosure that covered the entire measurement cavity and reduced the temperature fluctuations to $< 1\,^{\circ}C$ during measurements.

4.2 Interference by O_3

Although implementation of differential online and offline measurements theoretically accounts for all system baseline losses including those by O_3, we found that the presence of variable O_3 concentrations still caused significant interferences during measurements. The likely reason for these interferences was that high (> 10 ppb) O_3 concentrations caused high extinction ($\sim 1000\,Mm^{-1}$) losses reducing the CRDS sensitivity and affecting the exponential decay of the signal. Figure 7a shows measurements obtained during a day with natural O_3 spikes in ambient air. Absolute extinction in the cavity was strongly affected by increased O_3 concentrations as shown by a near-linear relationship between extinction and O_3 ($R^2 = 0.95$). Figure 7b shows O_3 concentrations also affected the differential measurements which theoretically only should be affected by extinction of GEM alone. To reduce interferences by O_3, we modified the ambient air inlet system to thermally decompose O_3 prior to measurements (Sect. 3.4) which allowed us to conduct ambient air measurements in the absence of O_3.

4.3 Frequency conversion efficiency

The final wavelength conversion of the laser system occurs in a frequency conversion unit (FCU) consisting of a barium borate (BBO) frequency doubling crystal that converts the fundamental dye laser wavelength from 507.3 nm to 253.65 nm. Standard protocol for the Sirah dye laser operation required calibrating the FCU motor position to the laser wavelength to reach optimal output power of the final wavelength. We achieved this by adjusting the position of the BBO crystal to maximize the laser peak power

AMTD
5, 8995–9020, 2012

across a wavelength range that encompassed the Hg absorption line; the FCU position was then entered into a calibration table. Linking the FCU position to the wavelength, however, meant that the FCU was adjusting position based on changes of the laser wavelength output which is not an accurate measurement of the real laser wavelength position (see above) and reflects long-term laser drifts (caused by temperature drifts or slow pressure changes within the laser, Demtröder, 2003). If we followed the standard protocol during measurements, we noticed that the frequency conversion efficiency of online and offline measurements changed, which caused large drifts in differential extinction measurements as online and offline measurements were affected differently by these drifts. As a result, we had to implement a mechanism to continuously adjust the FCU position in order to maintain equal wavelength conversion efficiencies for both wavelengths of the differential measurements.

We implemented a function in our LabVIEW control program to adjust the FCU position such that conversion efficiencies of online and offline measurements would not drift apart and remained stable during measurements. To do this, we continuously measured the signal power of online and offline pulses with the reference photodiode used for wavelength locking (Sect. 3.1). Using a 12-s moving average of the signal power of the differential pairs, we continuously adjusted the FCU position to minimize the difference in signal power between online and offline pulses (within 0.05 V as calculated with the online and offline signal measured by the PD_{Ref}).

5 Summary

We further developed a laboratory prototype CRDS system for continuous and automated operation for high time resolution measurements of GEM in ambient air. Changes included use of an external, isotopically enriched Hg cell for automated wavelength locking and stabilization to maintain laser wavelength on the peak absorption line of GEM; differential absorption measurements using a piezoelectric tuning element that allow for continuous accounting of system baseline extinction losses; modification

AMTD
5, 8995–9020, 2012

to data acquisition systems and software programs to acquire high-speed, ring-down data at 50 Hz frequency as well as process and analyze data in real time; installation in a mobile trailer; modification of inlet systems and temperature controls to minimize effects of changes in temperature and O_3; and control of the FCU to reduce drifts in the absolute extinction. The ambient air sensitivity that we calculated (0.35 ng m^{-3} at 5 min time resolution) showed that we were able to measure sub-ambient changes in GEM concentrations and demonstrated that the CRDS system can be compared to commercially-available and widely used sensors. In a subsequent paper, we describe in detail the performance of the CRDS system for GEM measurements in ambient air with comparison to a commercially-available analyzer (2537B Tekran; Pierce et al., 2012).

Acknowledgements. We would like to thank Nicholas Nussbaum for software development, Rick Purcell for technical assistance and engineering, and the facilities crew at the Desert Research Institute for help with the mobile trailer setup. We also acknowledge assistance of undergraduate student, Luke Arnone, and high school students, Juan Pablo Ponce de Leon and Quinn Campbell, in this research. The study was supported by a US National Science Foundation Major Instrumentation (NSF MRI) grant (NSF AGS Award #0923485).

References

Anderson, T. N., Magnuson, J. K., and Lucht, R. P.: Diode-laser-based sensor for ultraviolet absorption measurements of atomic mercury, Appl. Phys. B Lasers O., 87, 341–353, doi:10.1007/s00340-007-2604-z, 2007.

Arya, S. P. S.: Introduction to Micrometeorology, 2nd Edn., 2001, Academic Press, San Diego, 4–237, 2001.

Atkinson, D. B.: Solving chemical problems of environmental importance using cavity ring-down spectroscopy, Analyst, 128, 117–125, 2003.

Clarkson, T. W. and Magos, L.: The toxicology of mercury and its chemical compounds, CRC Cr. Rev. Toxicol., 36, 609–662, doi:10.1080/10408440600845619, 2006.

AMTD

5, 8995–9020, 2012

Deanna, L. D., Dieter, B., Brandi, C., and Anthony, J. H.: Temperature and pressure dependent rate coefficients for the reaction of Hg with Br and the reaction of Br with Br: a pulsed laser photolysis-pulsed laser induced fluorescence study, J. Phys. Chem. A, 110, 6623–6632, 2006.

Demtröder, W.: Laser Spectroscopy: Basic Concepts and Instrumentation, Springer Verlag, Berlin, Heidelberg, New York, 2003.

Donohoue, D. L., Bauer, D., and Hynes, A. J.: Temperature and pressure dependent rate coefficients for the reaction of Hg with Cl and the reaction of Cl with Cl: a pulsed laser photolysis-pulsed laser induced fluorescence study, J. Phys. Chem. A, 109, 7732–7741, 2005.

Edner, H., Faris, G. W., Sunesson, A., and Svanberg, S.: Atmospheric atomic mercury monitoring using differential absorption lidar techniques, Appl. Optics, 28, 921–930, 1989.

Faïn, X., Moosmüller, H., and Obrist, D.: Toward real-time measurement of atmospheric mercury concentrations using cavity ring-down spectroscopy, Atmos. Chem. Phys., 10, 2879–2892, doi:10.5194/acp-10-2879-2010, 2010.

Fitzgerald, W. F., Engstrom, D. R., Mason, R. P., and Nater, E. A.: The case for atmospheric mercury contamination in remote areas, Environ. Sci. Technol., 32, 1–7, doi:10.1021/es970284w, 1998.

Fritsche, J., Obrist, D., Zeeman, M. J., Conen, F., Eugster, W., and Alewell, C.: Elemental mercury fluxes over a sub-alpine grassland determined with two micrometeorological methods, Atmos. Environ., 42, 2922–2933, doi:10.1016/j.atmosenv.2007.12.055, 2008.

Griggs, M.: Absorption coefficients of ozone in the ultraviolet and visible regions, J. Chem. Phys., 49, 857–859, 1968.

Harris, R. C., Rudd, J. W. M., Amyot, M., Babiarz, C. L., Beaty, K. G., Blanchfield, P. J., Bodaly, R. A., Branfireun, B. A., Gilmour, C. C., Graydon, J. A., Heyes, A., Hintelmann, H., Hurley, J. P., Kelly, C. A., Krabbenhoft, D. P., Lindberg, S. E., Mason, R. P., Paterson, M. J., Podemski, C. L., and Robinson, A.: Whole-ecosystem study shows rapid fish-mercury response to changes in mercury deposition, Proc. Natl. Acad. Sci. USA, 104, 16586–16591, doi:10.1073/pnas.0704186104, 2007.

Huber, M. L., Laesecke, A., and Friend, D. G.: Correlation for the vapor pressure of mercury, Ind. Eng. Chem., 45, 7351–7361, doi:10.1021/ie060560s, 2006.

Inn, E. C. Y. and Tanaka, Y.: Absorption coefficient of ozone in the ultraviolet and visible regions, J. Opt. Soc. Am., 43, 870–872, 1953.

AMTD
5, 8995–9020, 2012

Jongma, R. T., Boogaarts, M. G. H., Holleman, I., and Meijer, G.: Trace gas-detection with cavity ring down spectroscopy, Rev. Sci. Instrum., 66, 2821–2828, 1995.
Lamborg, C. H., Fitzgerald, W. F., O'Donnell, J., and Torgersen, T.: A non-steady-state compartmental model of global-scale mercury biogeochemistry with interhemispheric atmospheric gradients, Geochim. Cosmochim. Ac., 66, 1105–1118, 2002.
Landis, M. S., Stevens, R. K., Schaedlich, F., and Prestbo, E. M.: Development and characterization of an annular denuder methodology for the measurement of divalent inorganic reactive gaseous mercury in ambient air, Environ. Sci. Technol., 36, 3000–3009, doi:10.1021/es015887t, 2002.
Lindberg, S., Bullock, R., Ebinghaus, R., Engstrom, D., Xinbin, F., Fitzgerald, W., Pirrone, N., Prestbo, E., and Seigneur, C.: A synthesis of progress and uncertainties in attributing the sources of mercury in deposition, AMBIO, 36, 19–32, 2007.
Lyman, S. N., Jaffe, D. A., and Gustin, M. S.: Release of mercury halides from KCl denuders in the presence of ozone, Atmos. Chem. Phys., 10, 8197–8204, doi:10.5194/acp-10-8197-2010, 2010.
Mauersberger, K., Barnes, J., Hanson, D., and Morton, J.: Measurement of the ozone absorption cross-section at the 253.7 nm mercury line, Geophys. Res. Lett., 13, 671–673, doi:10.1029/GL013i007p00671, 1986.
Molina, L. T. and Molina, M. J.: Absolute absorption cross sections of ozone in the 185- to 350-nm wavelength range, J. Geophys. Res., 91, 14501–14508, doi:10.1029/JD091iD13p14501, 1986.
Moosmüller, H., Varma, R., and Arnott, W.: Cavity ring-down and cavity-enhanced detection techniques for the measurement of aerosol extinction, Aerosol Sci. Tech., 39, 30–39, 2005.
Obrist, D., Hallar, A. G., McCubbin, I., Stephens, B. B., and Rahn, T.: Atmospheric mercury concentrations at Storm Peak Laboratory in the Rocky Mountains: evidence for long-range transport from Asia, boundary layer contributions, and plant mercury uptake, Atmos. Environ., 42, 7579–7589, doi:10.1016/j.atmosenv.2008.06.051, 2008.
Press, W. H., Flannery, B. P., Teukolsky, S. A., and Wetterling, W. T.: Numerical recipes: the art of scientific computing, 3rd edn., Cambridge University Press, Cambridge, New York, 1986.
Rothenberg, S. E., Mckee, L., Gilbreath, A., Yee, D., Connor, M., and Fu, X. W.: Evidence for short-range transport of atmospheric mercury to a rural, inland site, Atmos. Environ., 44, 1263–1273, doi:10.1016/j.atmosenv.2009.12.032, 2010.

AMTD
5, 8995–9020, 2012

Schroeder, W., Yarwood, G., and Niki, H.: Transformation processes involving mercury species in the atmosphere – results from a literature survey, Water Air Soil Poll., 56, 653–666, doi:10.1007/bf00342307, 1991.
Schroeder, W. H. and Munthe, J.: Atmospheric mercury – an overview, Atmos. Environ., 32, 809–822, 1998.
Schweitzer, J. W. G.: Hyperfine structure and isotope shifts in the 2537-Å line of mercury by a new interferometric method, J. Opt. Soc. Am., 53, 1055–1071, 1963.
Shia, R.-L., Seigneur, C., Pai, P., Ko, M., and Sze, N. D.: Global simulation of atmospheric mercury concentrations and deposition fluxes, J. Geophys. Res., 104, 23747–23760, doi:10.1029/1999jd900354, 1999.
Slemr, F., Schuster, G., and Seiler, W.: Distribution, speciation, and budget of atmospheric mercury, J. Atmos. Chem., 3, 407–434, doi:10.1007/bf00053870, 1985.
Spuler, S., Linne, M., Sappey, A., and Snyder, S.: Development of a cavity ringdown laser absorption spectrometer for detection of trace levels of mercury, Appl. Optics, 39, 2480–2486, 2000.
Swartzendruber, P. C., Jaffe, D. A., Prestbo, E. M., Weiss-Penzias, P., Selin, N. E., Park, R., Jacob, D. J., Strode, S., and Jaegle, L.: Observations of reactive gaseous mercury in the free troposphere at the Mount Bachelor Observatory, J. Geophys. Res.-Atmos., 111, D24301, doi:10.1029/2006jd007415, 2006.
Tao, S. Q., Mazzotti, F. J., Winstead, C. B., and Miller, G. P.: Determination of elemental mercury by cavity ringdown spectrometry, Analyst, 125, 1021–1023, 2000.
Unique features of the Tekran Model 2537B: available at: http://www.tekran.com/files/Tekran-2537B-Unique-Features.r103.pdf (last access: 11 January 2012), 2009.
Wheeler, M. D., Newman, S. M., Orr-Ewing, A. J., and Ashfold, M. N. R.: Cavity ring-down spectroscopy, faraday transactions, J. Chem. Soc., 94, 337–351, 1998.
Zhang, L., Wright, L. P., and Blanchard, P.: A review of current knowledge concerning dry deposition of atmospheric mercury, Atmos. Environ., 43, 5853–5864, doi:10.1016/j.atmosenv.2009.08.019, 2009.

AMTD
5, 8995–9020, 2012

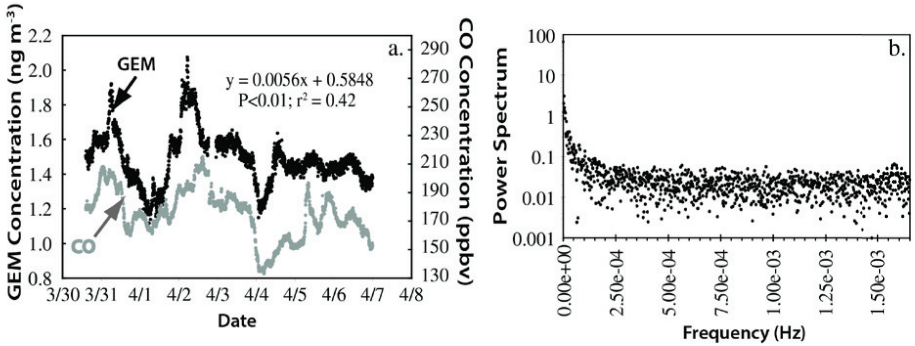

Fig. 1. (a) Time series of GEM over nine days of measurements (5 min time resolution) at Storm Peak Laboratory, Colorado with a conventional Tekran 2537 Hg analyzer and CO. **(b)** Power spectrum for GEM showing that the power spectrum does not drop at the Nyquist frequency (1.67×10^{-3} Hz).

AMTD
5, 8995–9020, 2012

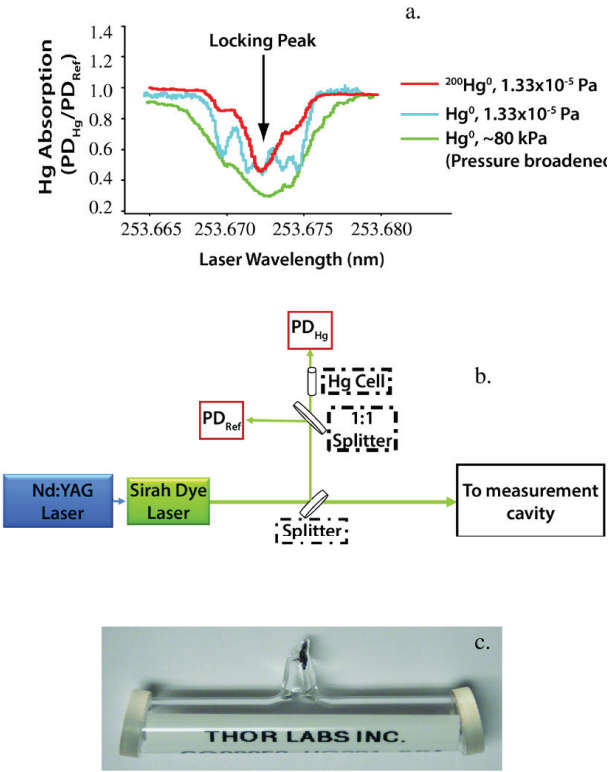

Fig. 2. (a) Absorption spectra of external Hg cells filled with metallic Hg (~ 80 kPa air and 1.33×10^{-5} Pa pressure Hg) and filled with isotopically-enriched ^{200}Hg at 1.33×10^{-5} Pa pressure. **(b)** Schematic diagram of the experimental setup including the Hg reference cell for control of laser wavelength. **(c)** External quartz cell filled with ^{200}Hg for wavelength locking of the laser system.

AMTD
5, 8995–9020, 2012

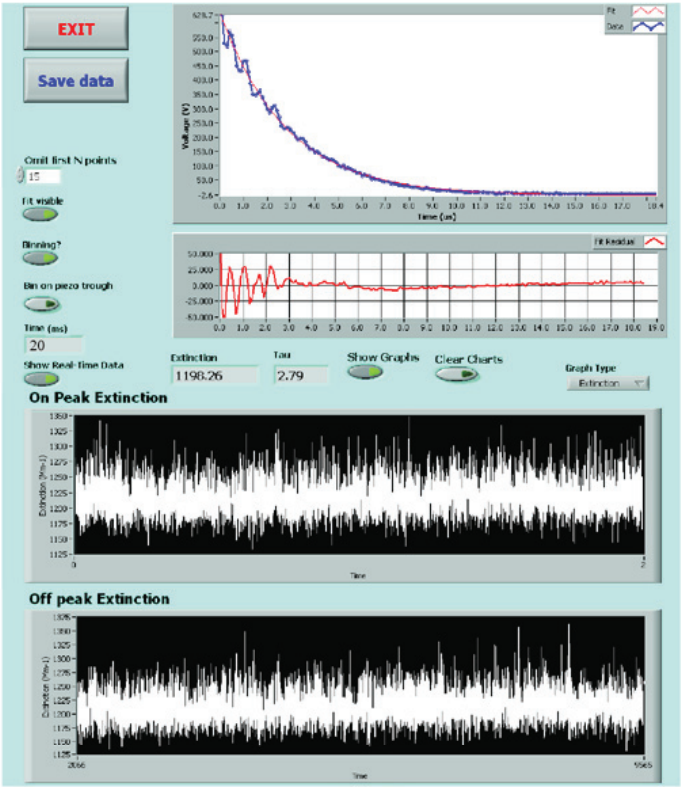

Fig. 3. LabVIEW interface with raw ring-down and residual graph. The first 15 points are omitted from the ring-down graph. Both online and offline extinction graphs are visible during operation to visualize separation of the two signals. The interface also displays the extinction and tau values at 50 Hz. The time box allows viewers to check that the program is acquiring data at 50 Hz (value should read 20 ms if this is the case).

AMTD
5, 8995–9020, 2012

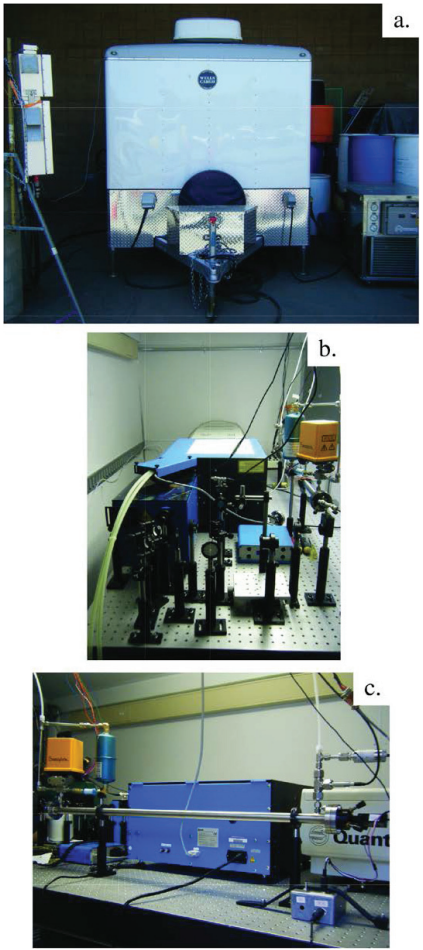

Fig. 4. (a) Mobile trailer and chiller setup at DRI. **(b)** Laser setup on optical table inside the mobile trailer. **(c)** CRDS cavity with laser in the background.

AMTD
5, 8995–9020, 2012

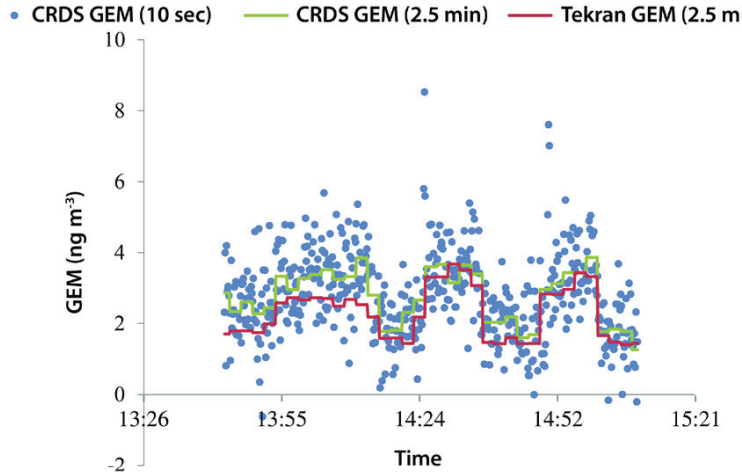

Fig. 5. Ambient air measurement for 1.5 h and comparisons of GEM measured by the CRDS system and a Tekran 2537B Hg analyzer (in ng m^3).

AMTD
5, 8995–9020, 2012

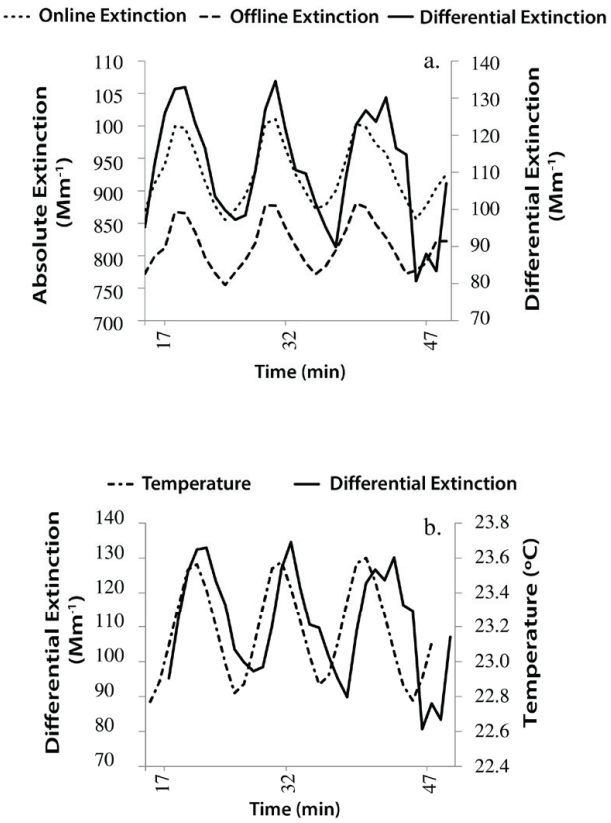

Fig. 6. (a) Online and offline absolute extinction signals and differential extinction as a function of time measured during an afternoon where we noticed significant temperature fluctuations (one min averaging time). **(b)** Differential extinction and corresponding temperature fluctuations during that afternoon (one min averaging time).

AMTD
5, 8995–9020, 2012

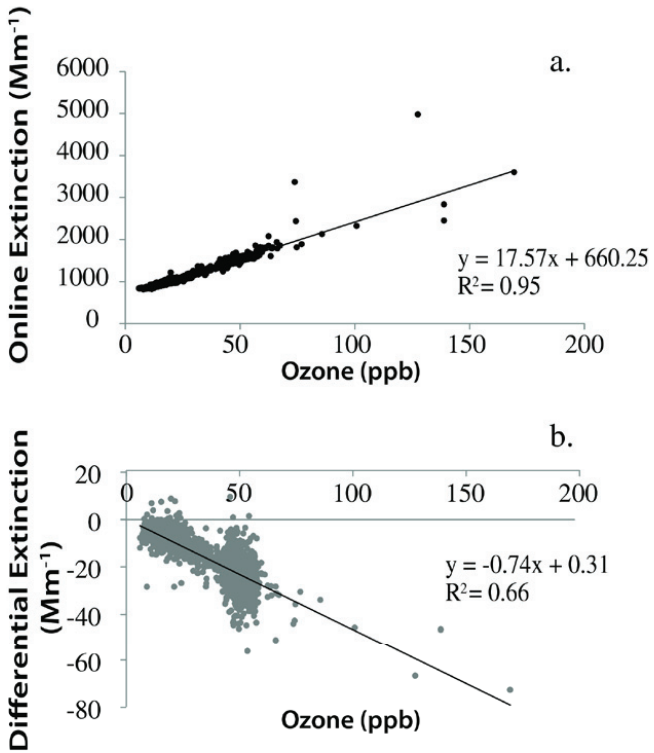

Fig. 7. (a) Online extinction as a function of O_3 concentration for one day of ambient air measurements with O_3 in sample stream (10 s averaging). Several natural spikes (up to 170 ppb) of O_3 occurred during measurements showing a slope of 17.57 Mm^{-1} per 1 ppb O_3 and an R^2 of 0.95. **(b)** Differential extinction as a function of O_3 concentration for one day of ambient air measurements with O_3 in sample stream (10 s averaging) showing a slope of −0.74 Mm^{-1} per 1 ppb of O_3 and an R^2 of 0.66.

AMTD
5, 8995–9020, 2012